Nanocellular Structures in Block Copolymers with CO_2-philic Blocks Using CO_2 as a Blowing Agent: Crossover from Micro- to Nanocellular Structures with Depressurization Temperature

Hideaki Yokoyama*,† and Kenji Sugiyama‡

Nanotechnology Research Institute, National Institute of Advanced Industrial Science and Technology, 1-1-1, Higashi, Tsukuba, Ibaraki 305-8564, Japan, and Department of Organic and Polymeric Materials, Graduate School of Science and Engineering, Tokyo Institute of Technology, 2-12-1, Ookayama, Meguro-ku, Tokyo 152-8552, Japan

Received August 8, 2005; Revised Manuscript Received October 5, 2005

ABSTRACT: Uniform nanocellular structures are successfully formed within the spherical nanodomains of CO_2-philic fluorinated blocks in Poly[styrene-*block*-4-(perfluorooctylpropyloxy)styrene] (PS−PFS) and Poly[styrene-*block*-perfluorooctylethyl methacrylate] (PS−PFMA) monoliths using supercritical (SC) carbon dioxide (CO_2). The nanocells have a very small surface area, indicative of the closed cell structure. Temperature of depressurization (T_d) is the key to the uniform nanocellular formation in the CO_2-philic block nanodomains: T_d must be well below the glass transition temperature (T_g) of the skeleton PS domains in the presence of CO_2. As T_d is raised and approaches T_g, the nanocellular structure crosses over to the microcellular structure on the order of micrometers, which is the typical cell structure formed via the conventional foaming mechanism. Two independent cell formation mechanisms coexist when T_d is in the vicinity of T_g. The nanocells have upper limit diameter of ca. 40 nm, which is apparently determined by the balance between the expansion of nanocells and diffusion of CO_2 either into the growing microcells or to the surface to evaporate. When T_d is set above T_g, we simply find conventional microcells only slightly smaller than those formed in homopolystyrene, which are indicative of the negligible effect of block copolymer nanodomains in the conventional process.

1. Introduction

Carbon dioxide (CO_2) is an environmentally friendly physical blowing agent widely used to introduce foams or cells in polymeric materials.[1] The typical cell size of such foams ranges from being on the order of micrometers to millimeters depending on CO_2 pressure, depressurizing temperature, solubility of CO_2 in polymers, and many other process dependent parameters.[2,3] Most polymeric materials do not dissolve in CO_2: hydrophobic polymers such as polyethylene,[4] polypropylene,[4] polystyrene,[5] poly(ethyl methacrylate)[6] and poly(methyl methacrylate)[6,7] are not soluble in CO_2 but are significantly swollen with CO_2.[8] In a conventional CO_2 process for microcellular foaming in such ordinary polymers, a polymer specimen is first swollen with CO_2 in a high pressure vessel, depressurized to atmosphere to foam. When necessary, the specimen is heated to a temperature above its glass transition temperature immediately after the rapid depressurization of CO_2. During rapid depressurization, solubility of CO_2 decreases with decreasing pressure, and then the oversaturated CO_2 in the polymer specimen nucleates and grows as bubbles in the CO_2-plasticized polymer specimen to form cellular or porous structures.[9,10] Nuclei of CO_2 in polymeric materials, in general, have a minimum diameter which is thermodynamically determined. Such minimum diameter is on the order of micrometers or just slightly below, and the number density of nuclei is small, e.g., 10^{10} cells/cm^3.[11] While CO_2 processes aiming to introduce smaller cellular structures into polymeric materials have been investigated for the past few decades,[1−4,12] fine-tuning of condition of the conventional CO_2 processes has limited capability to reduce the size of cells. Thermodynamics does not favor small nuclei, leading to a huge increment of the interfacial (surface) area and interfacial (surface) free energy.

Block copolymers are well-known for their self-assembling into nanoscopic periodic domain structures.[13] Such domains typically range from 5 to 100 nm, primarily depending on the molecular weight of block copolymers. Depending on asymmetry of the block fraction, block copolymers adopt a variety of ordered structures, such as spheres, cylinders, gyroids and lamellae. We focus on sphere-forming block copolymers, which provide well-ordered and densely packed spherical nuclei for nanobubbles and nanocellular structures. In order for spherical domains to work as nuclei for nanobubbling, those spherical domains must have a good affinity with CO_2 and the capability of localizing CO_2 in themselves. Fluorinated polymers are a class of CO_2-philic polymers, some of which are actually soluble in CO_2 above a certain CO_2 pressure;[8] block copolymers with fluorinated blocks are, therefore, potential candidates for nanobubbling.

Our group has just recently reported a successful fabrication of cellular structures with a uniform diameter of 10−30 nm and number density of 10^{16} cells/cm^3 in block copolymers with CO_2-philic fluorinated blocks using CO_2.[14,15] This methodology takes a full advantage of nanodomain structures of block copolymers, and uses them as templates to nucleate nanobubbles of CO_2 in such domains. The diameter of the cells using CO_2-foaming is much smaller, with monodisperse distribution, than those previously reported in the literature using polymer blends,[16] fine-tuning of temperature and

* To whom correspondence should be addressed. E-mail: yokoyama@ni.aist.go.jp.
† National Institute of Advanced Industrial Science and Technology.
‡ Tokyo Institute of Technology.

10.1021/ma051757j CCC: $30.25
Published on Web 11/15/2005

concentration of CO_2,[17] cross-linking of methacrylate in CO_2.[18] Poly(perfluorooctylethyl methacrylate) (PFMA) block was proved to be effective to localize CO_2 in its domains due to good solubility in CO_2. In the communications,[14,15] reducing depressurization temperature (T_d) down to 0 °C was necessary in order to freeze the continuous domain and to fix the CO_2-swollen PFMA domains before depressurization. We study the effect of T_d on the cell size and distribution, and we explore the possibility of controlling the cell size from nano- to micrometer scales.

2. Experiments

Polymer Synthesis and Sample Preparation. Poly[styrene-*block*-perfluorooctylethyl methacrylate] (PS−PFMA) was synthesized via sequential anionic polymerization of styrene and perfluorooctylethyl methacrylate in tetrahydrofuran (THF) at −78 °C and characterized as described previously.[19] Poly[styrene-*block*-4-(perfluorooctylpropyloxy)styrene] (PS−PFS) block copolymers were polymerized by the following steps. First, polystyrenes were polymerized by *sec*-butyllithium as an initiator in THF at −78 °C in high vacuum. The living polystyryllithium was subsequently reacted with 4-hydroxystyrene protected by *tert*-butyldimethylsilane (TBDMS) to form poly[styrene-*block*-4-*tert*-butyldimethylsilyloxy)styrene] (PS−PSOTBDMS) followed by termination with methanol. PS−PSOTBDMS was deprotected in THF by adding hydrochloric acid to form poly(styrene-*block*-4-hydroxystyrene) (PS−PSOH). Williamson reaction was used to introduce 1-bromo-3-perfluorooctylpropane into PSOH to obtain PS−PF copolymers. The detail of the synthesis, the polymerization and the characterization have been described elsewhere.[19,20] The molecular weights of the PS blocks were measured by gel permeation chromatography (GPC) with PS standards. The weight fractions of the PF blocks, f_{PFS} and f_{PFMA} were measured by ^{1}H NMR and estimated with assumed density of perfluorooctyl group of 1.6. The polydispersities of PS−PFS and PS−PFMA copolymers are less than 1.1. PS−PFS and PS−PFMA were dissolved in a mixture of 80 wt % of toluene (Wako Pure Chemical Industries, Ltd.) and 20 wt % of 1,1,1,3,3,3-hexafluoro-2-propanol (Wako Pure Chemical Industries, Ltd.). Thick films were cast from the solution and vacuum-dried at room temperature for 12 h.

CO_2 Processing. A stainless steel high-pressure vessel for CO_2 processing was connected to a high-pressure liquid chromatography pump (JASCO PU-2086 plus) with a cooling head, and to a back-pressure regulator (JASCO SCF−Bpg). Films of PS−PF were placed in the high-pressure vessel and annealed at 60 °C for 1 h with a constant pressure controlled using the pressure regulator. We have preannealed some specimens in a vacuum oven at 160 °C for 10 h, but the morphology and final cellular structures remain unchanged. Because of that, we processed the specimens without thermal annealing. The vessel was placed in a temperature-controlled water bath to quench the films to a desired temperature while maintaining the pressure using the pump and regulator. Immediately after the vessel reached a desired temperature, the CO_2 pressure was slowly reduced. The depressurization rate was controlled at 0.5 MPa/min for all experiments otherwise stated.

Scanning Electron Microscopy (SEM). Films are fractured in liquid nitrogen to expose the internal cellular structures to the surface. Structures on the cryo-fractured surfaces were observed using an environmental scanning electron microscope (ESEM) (Phillips XL20 ESEM-FEG) equipped with a field emission gun. 5 to 6 keV of electron beam was used for the observation with working distance of less 10 mm. To avoid a possible artifact, no conductive coating was employed. To avoid a possible electric charge buildup without conductive coating, ca. 0.8 Pa of water vapor was introduced in the sample chamber of the ESEM. The secondary electrons (SE) are detected and imaged with environmental secondary detector (ESD) in the presence of water vapor. ESD takes full advantage of the ionization of water vapor, which is induced by the interaction of SE and water molecule.[21] The ionization of water results in the cascading multiplication of the SE intensity. Therefore, adding water vapor significantly enhances the sensitivity while too high vapor pressure deteriorates the resolution somewhat. By fine-tuning of the energy of incident electron and vapor pressure of water, the porous structures of the diameter down to 20 nm can be successfully imaged without the use of conducting coating. The low-pressure mode of an ESEM equipped with a field emission gun is an ideal tool for observing nanoporous polymeric (insulating) materials.

Surface Area Measurement. The surface area of the selected PS−PFMA nanocellular monolith was quantified by Kr gas adsorption porosimetry using a Micrometrics ASAP 2020 gas adsorption instrument, and the data were manipulated using the software supplied with the instrument. Specific surface calculation of membranes was carried out by the Brunauer−Emmett−Teller (BET) method. For the adsorption measurement, Kr instead of N_2 was used for BET surface area measurement since Kr is more sensitive than N_2 to small surface areas.

3. Results

It has long been known that CO_2 can be used as a physical blowing agent for a wide variety of polymeric foams. In the "conventional" process using CO_2, a polymer specimen is immersed in CO_2 followed by rapid depressurization at a temperature around or slightly below the glass transition temperature (T_g) of the polymer but above the T_g of the polymer in the presence CO_2. We first test the applicability of the conventional process for producing cells in nanometer order (nanocells) using block copolymers with CO_2-philic blocks, which are expected to work as templates for nanocellular formation. Monoliths of poly[styrene-*block*-4-(perfluorooctylpropyloxy)styrene] (PS−PFS) with a weight-average molecular weight, M_w, of 94 000 g mol^{-1} and PFS volume fraction, f_{PFS}, of 0.23 and polystyrene (PS) with M_w of 99 000 g mol^{-1} are immersed in CO_2 of a pressure of 20 MPa at temperatures ranging from 80 to 107 °C for 1 h. CO_2 pressure was reduced rapidly (in a few seconds) so that CO_2 expands in the plasticized copolymer matrices, and then the expanded cells are fixed by the glass transition of PS. Regardless of our expectation, the monoliths turned white after the process, indicating microcellular formation. The diameters and distributions of the cells of the monoliths processed at different temperatures were determined by scanning electron microscopy (SEM) after the monoliths were frozen in liquid nitrogen and fractured to expose the internal structures to the surfaces. The average diameters and standard deviations of cells are plotted in Figure 1. The cells in PS−PFS are slightly (about a factor of $^1/_2$) smaller than those in PS. Despite the expectation that the PFS domains may work as a template of foams and nucleate nanofoams, the size reduction achieved using PS−PFS is negligibly small. It has been known that polymers highly swollen with CO_2 produce smaller cells due to the higher degree of oversaturation and to the larger number of nuclei formed in the initial stage of the foaming process. The size reduction of cells in PS−PFS relative to PS seems solely due to the higher degree of absorption of the CO_2-philic PFS blocks: the nanodomains of PFS do not simply work as nuclei in the foaming process. By reducing saturation and depressurization temperatures, the size of cells goes barely below 1 μm in diameter in PS−PFS monoliths. Consequently, the conventional process controls the size of cells in the micrometer range

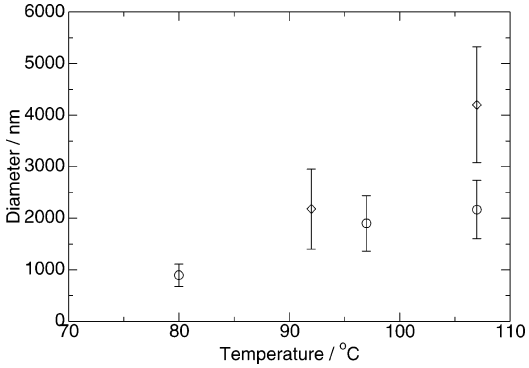

Figure 1. Dependence of the diameter of cells in the polystyrene (diamond) and PS−PFS block copolymer (circle) monoliths on processing (saturation and depressurization) temperature.

but does not lead to nanocellular structures even using the block copolymers with CO_2-philic blocks. Reducing temperature further down to below 80 °C combined with rapid depressurization causes occasional crack in the specimens. The large pressure gradient upon rapid depressurization, solidified CO_2 due to the latent heat of evaporation and brittle polymer monoliths at lowered temperature are presumably the main reasons; therefore, we cannot extend this strategy (rapid depressurization) to reduce the accessible cell size.

Instead of extending the conventional processes, the step of reducing depressurization temperature, T_d, to 0 °C followed by slow depressurization was proved to be the essential step for the successful fabrication of nanocellular structures, as reported in our previous communications.[14,15] Reducing T_d to 0 °C prevents the growth of the cells filled with CO_2 even with fairly slow depressurization, i.e., 0.5 MPa/min. It is essentially a "nucleation only" process with the help of block copolymer nanodomains opposed to the conventional "nucleation and growth". PS continuous domains become glassy at T_d of 0 °C, and the size of the cells is successfully controlled by the saturation pressure of CO_2 within the range of 10−30 nm. We, therefore, investigated the effect of T_d to test the ultimate control of the size of the nanocells. In our previous study, polystyrene-*b*-perfluorooctylethyl methacrylate (PS−PFMA) with M_w of 33 000 and a volume fraction of PFMA, f_{PFMA}, of 0.29 was used for a template of nanocellular structures. We confirm that the nanocellular structures can also be introduced in PS−PFS used in this study with the different backbone chemical structures and higher molecular weights, but with the same perfluorooctyl side group. An example of the nanocellular structures formed in PS−PFMA monoliths is observed by SEM and shown in Figure 2a. The specimen was saturated with CO_2 at 60 °C and cooled to 0 °C prior to the depressurization process. We reconfirm the similar appearance of nanocells in the PS−PFMA monolith, and the same processing method was applied to PS−PFS. An SEM picture of cryo-fractured surface of PS−PFS is shown in Figure 2b. The structure is almost identical to the SEM picture in Figure 2a but the nanocells seem to be separated with thicker walls apparently due to higher M_w and smaller f_{PFS} of PS−PFS. Domain spacings of PS−PFMA and PS−PFS are estimated from the first-order peaks of the FFTs of the corresponding SEM images. The domain spacing of PS−PFS was estimated to be 47 nm, which is slightly larger than 42 nm of PS−PFMA. The difference is qualitatively consistent with the molecular

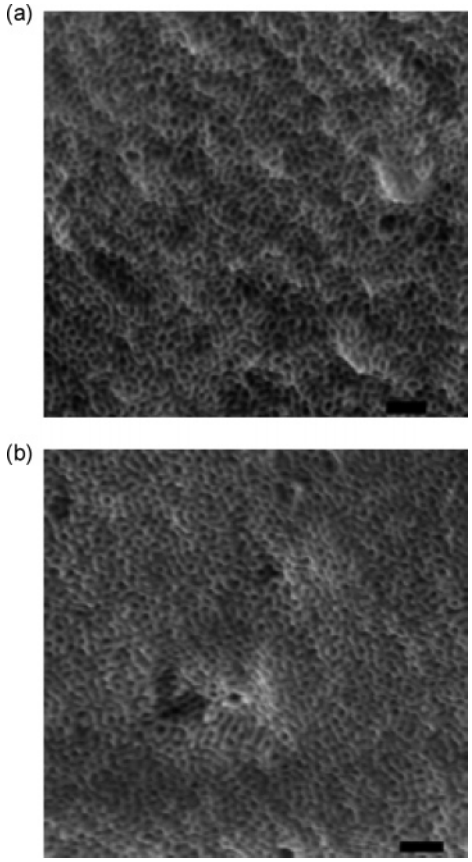

Figure 2. SEM images of nanocellular PS−PFMA (a) and PS−PFS (b) monoliths saturated at 30 MPa and 60 °C, and then depressurized at 0 °C at a rate of 0.5 MPa/min. The bars indicate 200 nm.

weights of PS−PFMA and PS−PFS. The <10% difference of the spacings is rather small relative to the difference of the molecular weights by a factor of 3 (94 000 for PS−PFS and 33 000 for PS−PFMA). Since PS−PFMA with higher fluorinated block fraction is expanded by CO_2 with a higher degree, the resultant spacing is determined not only by the molecular weights but also by the fluorinated block fraction and its solubility in CO_2. It is, however, clearly indicated that the solubility of CO_2-philic block in CO_2 is the key factor for nanocellular fabrications and that the methodology can be applicable for some other CO_2-philic polymer species.

We believe that the nanocells in the monoliths at low expansion rate are independent closed cells according to the apparent mechanism of cell formation—the CO_2 droplets are emulsified by the PS−PFMA or PS−PFS and stabilized before the gentle removal of CO_2. To confirm the independence of the nanocells, we evaluated the surface area of the monoliths. If the nanocells are not closed cells but open pores, a large surface area should be observed. We performed a BET adsorption experiment with Kr gas on the PS−PFMA monoliths. The isotherm at liquid nitrogen temperature is plotted as a function of relative pressure, P/P_o, in Figure 3. The monoliths are frozen by liquid nitrogen and fractured into small pieces before the adsorption experiment so that the cells or pores are exposed to the fractured surfaces. By analyzing the adsorption isotherm using the BET method, we obtain a surface area of 0.0509 m^2/g. As seen in Figure 3, the adsorption behavior is conventional and the BET plot gave a straight line (not

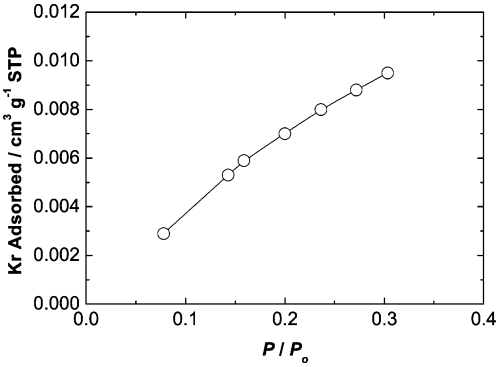

Figure 3. Kr adsorption isotherm for the nanocellular PS−PFMA monoliths that was saturated at 30 MPa and 60 °C, and then depressurized at 0 °C at a rate of 0.5 MPa/min.

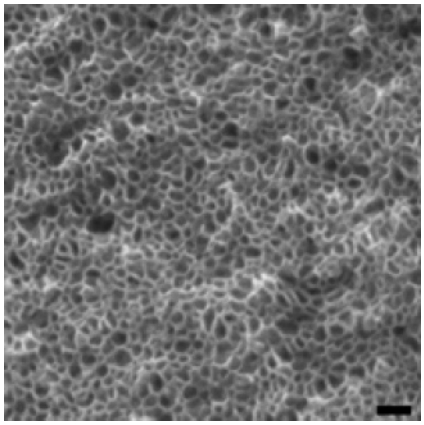

Figure 4. SEM image of a microcellular PS−PFS monolith processed at 60 °C and 30 MPa and depressurized at 25 °C at a rate of 0.5 MPa/min. The bar indicates 200 nm.

shown here), but the obtained BET surface area is very small considering the nanostructure. For instance, porous divinylbenzene resins exhibit well over 500 m^2/g N_2 BET surface area due to their connected porous morphology.[22] The difference of 4 orders of magnitude in the BET surface areas clearly confirms that the nanocellular structures in the PS−PFMA monoliths processed by our CO_2-method have closed nanocells.

We are interested in expanding the range of size accessible to our block copolymers without changing the molecular structure. We raised the temperature of the CO_2 depressurization process (T_d) from 0 up to 40 °C in order to control the size of the cells while maintaining the other controlling parameters. The detail of the experimental process is described in the Experimental Section. Since the viscosity of PS domains swollen with CO_2 is reduced at elevated temperature, we expect that the cell size increases as a result of expansion of the cells with increasing T_d. An SEM image of PS−PFS quenched to 25 °C followed by depressurization at 0.5 MPa/min is shown in Figure 4. The size of cells depressurized at 25 °C is significantly larger than that at 0 °C. The cells are still closed, but the distribution of cell size is significantly broader. The wall separating cells apparently become thin relative to the cell size compared to that depressurized at 0 °C. Unfortunately, we were not able to measure mass densities of those specimens due to a limited amount of copolymer, but the mass density should be significantly reduced by depressurization at elevated temperature since the larger cells are surrounded with thin walls through visual inspection of the SEM image in Figure 4. An SEM

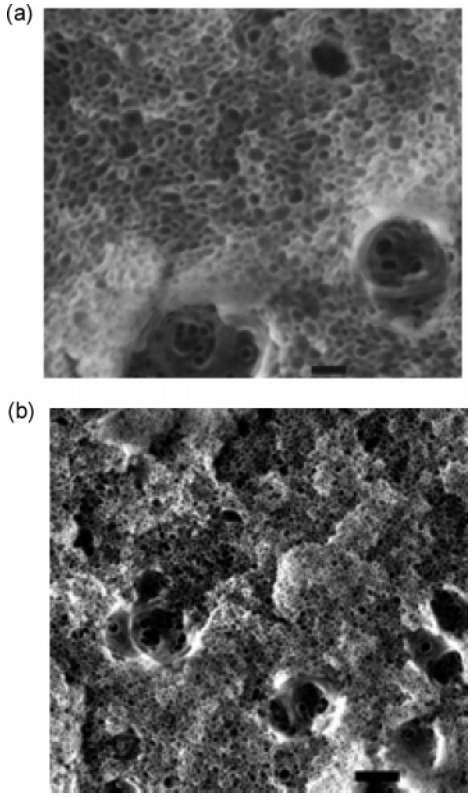

Figure 5. SEM images of a nano- and microcellular PS−PFS monolith processed at 60 °C and 30 MPa and depressurized at 32 °C at a rate of 0.5 MPa/min with the scale bars of 200 nm (a) and 500 nm (b).

image of PS−PFS quenched to 32 °C followed by depressurization at 0.5 MPa/min is shown in Figure 5 with two different magnifications. As T_d is further increased to 32 °C, we start to find the larger cells (>500 nm) surrounded by the smaller cells (<100 nm): the size distribution is apparently bimodal. Let us call those larger and smaller cells microcells and nanocells, respectively. At a CO_2 pressure of 30 MPa, T_d of 32 °C is close to the reduced glass transition temperature of PS swollen by CO_2. T_g ranges from 31 °C (at 25 °C) to 42 °C (at 45 °C) depending on temperature.[23] The temperature dependent T_g is due to temperature-dependent plasticization of PS with CO_2: PS absorbs more CO_2 and indicates lower T_g at lower temperature. The larger cells in Figure 5 may thus be formed by the kinetics of microcellular formation widely observed in CO_2-swollen homopolymers depressurized above their glass transition temperatures. Once nuclei of microcells are formed in the block copolymer, CO_2 diffuse into the cells as decreasing solubility in the polymer with decreasing pressure. On the interior of the large cells, small nanocells appear to be connected: the growing microcells apparently destroy and absorb the nanocells. T_d is further increased to 40 °C, which is proximity of the reduced glass transition temperature of PS in the presence of CO_2 at 30 MPa. We observed the center of the specimen far away from the surfaces, and found many microcells as shown in Figure 6a. Some of the cells reach 1 μm in diameter; however, we still find the nanocells surrounding the microcells. The distribution is again evidently bimodal similar to the structure obtained at T_d of 32 °C. When we focused onto the near surface area of the specimen, we found no microcells developing as shown in Figure 6b. The absence of microcells near the surface is evidently typical skin

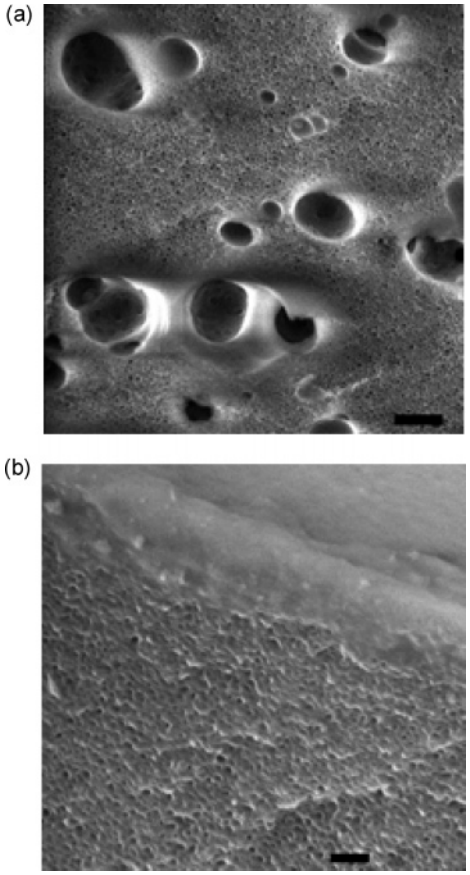

Figure 6. SEM images of a cellular PS−PFS monolith processed at 60 °C and 30 MPa and depressurized at 40 °C at a rate of 0.5 MPa/min in bulk (a) with a scale bar of 500 nm and near the surface (b) with a scale bar indicating 200 nm. The surface is smooth and no pores are found.

formation observed in micro- and macrocellular formation, in which CO_2 diffuses and evaporates from the surface without foaming cells. It should be noted that such skin formation and microcellular formation, which are typical in conventional foaming in polymeric materials, are observed even in the presence of the nanocells. The nano- and microcellular formations appear to be independent and to be based on completely different mechanisms.

4. Discussion

The size distributions of the nanocells that are defined as the cells <100 nm are plotted in Figure 7. The statistics excludes the microcells. At 0 °C, we find a narrow distribution of nanocells of an average size of 20 nm. This process is the same as the process in our communications reporting a successful fabrication of nanocells in polymeric monoliths[14] and thin films.[15] As T_d increases to 25 °C, the average size increases to 40 nm and the distribution becomes broad. It should be noted that, at this temperature, we did not find microcellular formation as already shown in Figure 6. The size control of nanocells by elevating T_d to 25 °C is hence successful while the size distribution is significantly broader. With further increasing T_d, the cell diameter does not increase but rather decreases at T_d of 30 °C or above. The cell diameter becomes maximum at $T_d = 30$ °C, which roughly agrees with the T_g of PS in CO_2 at a pressure of 30 MPa.[23] When T_d is close to but still below the T_g of PS, nanocells are expanded by the combination of pressure gradient and reduced stiffness of PS with

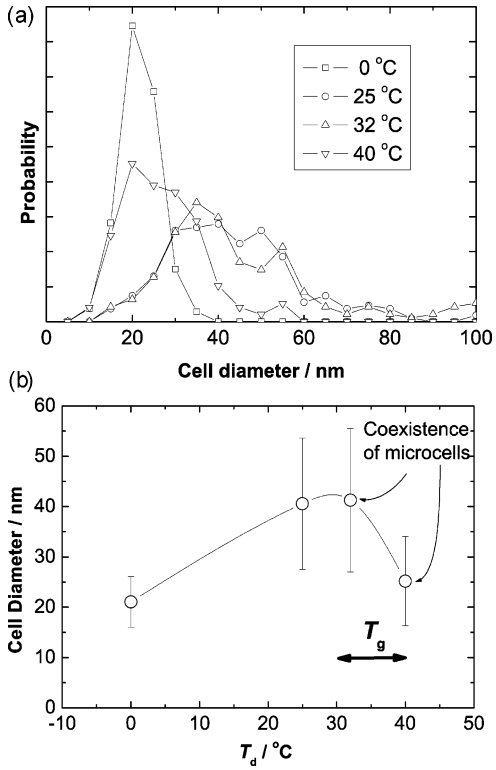

Figure 7. (a) Size distribution of nanocells in a variety of depressurization temperatures. Microcells are excluded from the statistics and the cells less than 100 nm in diameter were counted. (b) Dependence of cell diameter on depressurization temperature. The horizontal arrow indicates the range of T_g of polystyrene in 30 MPa of CO_2. T_g depends on temperature due to temperature-dependent plasticization. Near this reduced T_g or above, coexistence of nano- and microcells is found.

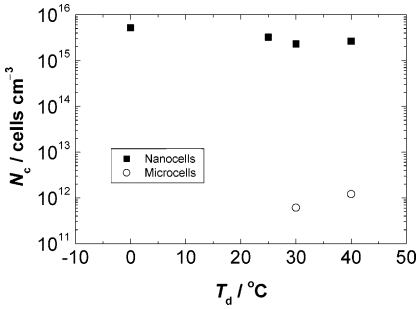

Figure 8. Dependences of the number densities (N_c) of nanocells and microcells on depressurization temperature (T_d). Density of nanocells (<100 nm) is the local density in the region where no microcells (>100 nm) are observed.

increasing T_d. The size of the nanocells, however, does not increase any further when T_d is above the T_g of PS in the presence of CO_2.

The number densities, N_c, of nanocells and microcells are plotted as a function of T_d in Figure 8. The density of nanocells is defined as the local number density in which the volume of microcells is excluded. The density of the nanocells is the order of 10^{15} cells cm^{-3} and several orders of magnitude larger than that of a typical microcellular foams. The T_d dependence is surprisingly small in this temperature range. The microcells start to appear at the T_g of PS in CO_2 and their number density is the order of 10^{11} to 10^{12}, a typical number density of microcellular formation. We speculate and illustrate in Figure 9 on a possible mechanism of this unique dependence of cell diameter and number density on temperature. The oversaturated CO_2 upon depres-

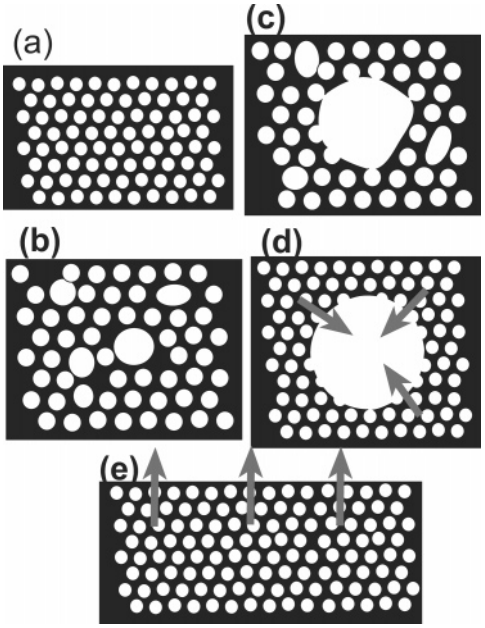

Figure 9. Schematic illustrations of nanocellular formations depressurized at T_d well below the T_g of PS in CO_2 (a), i.e., $T_d \ll T_g$, $T_d < T_g$ (b), $T_d = T_g$ (c), $T_d > T_g$ in bulk (d) and $T_d > T_g$ near the surface (e). Microcells begin to form at approximately T_g. nanocells do not expand at T_d above T_g in CO_2 since the pressure in the nanocells are released by diffusion of CO_2 (d) into the microcells or surface (e).

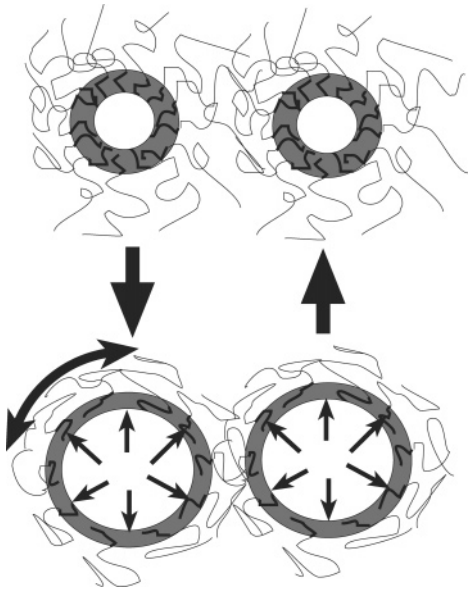

Figure 10. Schematic illustration of expanding nanocells in block copolymer nanodomains and elastic forces acting on the cells. Pressure in the cells expands the cells, stretches block copolymer domains in the peripheral direction and compress block copolymer chains in the radial direction. If the number of chains per cell does not change, the elastic force of a block copolymer "balloon" resists being expanded and limits the size of cells.

surization expands nanocells as observed in the monoliths depressurized at 0−25 °C, at which diffusion of CO_2 is limited and the matrix polymer is still glassy. It appears that even at a temperature below the T_g of PS in CO_2, the cells can expand some degree as illustrated in Figure 9, parts a and b. With increasing temperature, nanocells do not expand any further but the microcells start to form and to coexist with the nanocells (Figure 9c). Further increasing temperature above the T_g of PS in CO_2 at a pressure of 30 MPa, many microcells form in bulk. In such a case, oversaturated CO_2 diffuses into and expand the microcells as schematically shown in Figure 9d, and hence the residual pressure of CO_2 in the nanocells decreases. A similar behavior is found near the surface. The rapid CO_2 diffusion and evaporation form the surface prevent the nucleation and growth of microcells as well as expansion of nanocells. Consequently the residual pressure to expand the nanocells is reduced either in bulk by coexisting with microcells or near the surface by diffusion and evaporation.

Why does not the size of nanocells grow any further at a temperature above the T_g of PS? The diameter even decreases when microcells begin to appear. We illustrate a possible mechanism of the prevention of cell growth and shrinking of nanocells in Figure 10. Since expansion of the nanocells occurs in a short time scale during depressurization relative to the slow relaxation time of block copolymers[24] (relaxation of aggregation number), it is a good assumption that the number of block copolymer chains surrounding a nanocell remains constant during the depressurization process. Fluorinated block is not only partitioned at the surface to reduce the surface tension[25] but also strongly attracted to the CO_2 interface;[26] the interior of the cells is expected to be covered by the fluorinated blocks as shown in Figure 10. When the nanocells are expanded in the nanodomains, the surrounding PFS domains (and equivalently PS domains) are stretched in the peripheral direction and thus the block copolymer chains are significantly compressed in the radial direction. Such compression of block copolymer chains stores elastic energy and resists the expansion of the cells. This elastic energy prevent the nanocells expanding further and shrinks the cells when the internal pressure is lost. If the internal pressure in the nanocells is lost by the diffusion of CO_2 either to the microcells or surface, this stored elastic energy as well as the surface tension of the interior of the cells shrinks the nanocells.

5. Summary

We confirmed that successful fabrication of nanocellular structures using two different block copolymers. The closed cell structures are confirmed by adsorption measurement. Depressurization temperature is important for nano- and microcellular formation in fluorinated block copolymers using CO_2. Nano- and microcellular formations are independent processes and provide a bimodal cell distribution. When the temperature is near the glass transition temperature of continuous domains, microcells start to appear and coexist with nanocells in the fluorinated spherical domains, whereas nanocells exclusively form at a temperature well below the T_g of PS in the presence of CO_2. The expansion of nanocells at elevated temperature does not reach microcells apparently because the block copolymer domains surrounding the nanocells are stretched and resist for the expansion of the cells. The remaining CO_2 in the rubbery matrix rather leads to microcellular formation similar to the conventional CO_2 process and to bimodal distribution of the cell size.

Acknowledgment. This research has been partially funded by the Project on Nanostructured Polymeric Materials by the New Energy and Industrial Technology Development Organization.

References and Notes

(1) Cooper, A. I. *Adv. Mater.* **2003**, *15*, 1049.
(2) Han, X. M.; Koelling, K. W.; Tomasko, D. L.; Lee, L. J. *Polym. Eng. Sci.* **2003**, *43*, 1206.
(3) Goel, S. K.; Beckman, E. J. *Polym. Eng. Sci.* **1994**, *34*, 1137.
(4) Shieh, Y. T.; Su, J. H.; Manivannan, G.; Lee, P. H. C.; Sawan, S. P.; Spall, W. D. *J. Appl. Polym. Sci.* **1996**, *59*, 695.
(5) Zhang, Y.; Gangwani, K. K.; Lemert, R. M. *J. Supercrit. Fluids* **1997**, *11*, 115.
(6) Condo, P. D.; Johnston, K. P. *J. Polym. Sci., Part B, Polym. Phys.* **1994**, *32*, 523.
(7) Goel, S. K.; Beckman, E. J. *Polymer* **1993**, *34*, 1410.
(8) O'Neill, M. L.; Cao, Q.; Fang, M.; Johnston, K. P.; Wilkinson, S. P.; Smith, C. D.; Kerschner, J. L.; Jureller, S. H. *Ind. Eng. Chem. Res.* **1998**, *37*, 3067.
(9) Sun H. L.; Mark, E. J. *J. Appl. Polym. Sci.* **2002**, *86*, 1692.
(10) Goel, S. K.; Beckman, E. J. *Polym. Eng. Sci.* **1994**, *34*, 1148.
(11) Sun, X.; Liu, H.; Li, G.; Liao, X.; He, J. *J. Appl. Polym. Sci.* **2004**, *93*, 163.
(12) Sun, H.; Mark, J. E.; Tan, S. C.; Venkatasubramanian, N.; Houtz, M. D.; Arnold, F. E.; Lee, C. Y.-C. *Polymer* **2005**, *346*, 6623. Siripurapu, S.; Coughlan, J. A.; Spontak, R. J.; Khan, S. A. *Macromolecules* **2004**, *37*, 9872. Siripurapu, S.; DeSimone, J. M.; Khan, S. A.; Spontak, R. J. *Macromolecules* **2005**, *38*, 2271.
(13) Bates, F. S.; Fredrickson, G. H. *Annu. Rev. Phys. Chem.* **1990**, *41*, 525.
(14) Yokoyama, H.; Li, L.; Nemoto, T.; Sugiyama, K. *Adv. Mater.* **2004**, *16*, 1542.
(15) Li, L.; Yokoyama, H.; Nemoto, T.; Sugiyama, K. *Adv. Mater.* **2004**, *16*, 1226.
(16) Krause, B.; Diekmann, K.; van der Vegt, N. F. A.; Wessling, M. *Macromolecules* **2002**, *35*, 1738.
(17) Krause, B.; Sijbesma, J. J. P.; Munuklu, P.; van der Vegt, N. F. A.; Wessling, M. *Macromolecules* **2001**, *34*, 8792.
(18) Hebb, A. K.; Senoo, K. Bhat, R.; Cooper, A. I. *Chem. Mater.* **2003**, *15*, 2061.
(19) Sugiyama, K.; Nemoto, T.; Koide, G.; Hirao, A. *Macromol. Symp.* **2002**, *181*, 135.
(20) Hirao, A.; Koide, G.; Sugiyama, K. *Macromolecules* **2002**, *35*, 7642.
(21) Baumgarten, N. *Nature (London)* **1989**, *341*, 81.
(22) Macintyre, F. S.; Sherrington, D. C. *Macromolecules* **2004**, *37*, 7628.
(23) Wang, W.-C. V.; Kramer, E. J.; Sachse, W. H. *J. Polym. Sci., Polym. Phys. Ed.* **1982**, *20*, 1371.
(24) Yokoyama, H.; Kramer, E. J. *Macromolecules* **1998**, *31*, 7871.
(25) Yokoyama, H.; Tanaka, K.; Takahara, A.; Kajiyama, T.; Sugiyama, K.; Hirao, A. *Macromolecules* **2004**, *37*, 939.
(26) Yokoyama, H.; Sugiyama, K. *Langmuir* **2004**, *20*, 10001.

MA051757J